Supporting Information

Observational insights into aerosol formation from isoprene

David R. Worton[1,2], Jason D. Surratt[3], Brian W. LaFranchi[4,a], Arthur W. H. Chan[1], Yunliang Zhao[1], Robin J. Weber[1], Jeong-Hoo Park[1,c], Jessica B. Gilman[5,6], Joost de Gouw[5,6], Changhyoun Park[7,b], Gunnar Schade[7], Melinda Beaver[8,d], Jason St. Claire[8], John Crouse[8], Paul Wennberg[8], Glenn M. Wolfe[9,e], Sara Harrold[9], Joel A. Thornton[9], Delphine K. Farmer[5,10,f], Kenneth S. Docherty[5,10,g], Michael J. Cubison[5,10,h], Jose-Luis Jimenez[5,10], Amanda A. Frossard[11], Lynn M. Russell[11], Kasper Kristensen[12], Marianne Glasius[12], Jingqiu Mao[13], Xinrong Ren[14], William Brune[15], Eleanor C. Browne[4, i], Sally E. Pusede[4], Ronald C. Cohen[4], John H. Seinfeld[16] and Allen H. Goldstein[1,17].

Contents

SI text

1.1 Experimental Methods

1.1.1 Filter Collection

Filter samples (33 in total including two field blanks; 16 in 2007 and 17 in 2009) were collected on quartz fiber filters (Gellman QM-A) using a Thermo Anderson Total Suspended Particulate (TSP) high-volume sampler with an SA-230-F impaction plate at a volumetric flow of 68 m^3 hr^{-1} yielding a sample cutpoint of 2.5 microns ($PM_{2.5}$). Samples were collected for either 6 (morning; 7am – 1pm; afternoon, 1pm – 7pm) or 12 hours (night, 7pm – 7am at 9.3 m on the main north tower for two continuous five day periods from September 20^{th} – 25^{th} in 2007 and July 26^{th} – 31^{st} in 2009 *(1)*. As the filter samples were collected in the later period of the 2007 campaign, only supporting data from that period will be used in this paper unless otherwise stated. A comparison of the temperature, relative humidity, photosynthetically active radiation, organic and sulfate aerosol loadings during the filter collection periods for both campaigns are shown in Figure S5.

1.1.1 OH Measurements

OH and HO_2 were measured at various heights between 2 and 15m from a movable lift adjacent to the main north tower. Vertical profiling was conducted two to three times per day but the majority of the time the lift was kept at a height of 9, 12, or 15 m. As little variability was found for OH, HO_2 and OH reactivity at these three heights (less than 20 %), we use all the measurements from these three heights to ensure sufficient datapoints *(2)*. In 2009, OH was also measured by chemical modulation using the signal difference with and without the addition of high-purity gaseous perfluoropropene (C_3F_6) that removes OH prior to detection by LIF (OHchem) *(2)*. Mao et al., *(2)* showed that internally generated interferences lead to an overprediction of OH concentrations by the OHwave method. They also observed a positive temperature dependence in the difference between the two methods, which was used to correct the OHwave measurements used in this work.

1.2 Acyl peroxy nitrates (APNs) steady state model

The APN model employed in this work has been described in detail by Lafranchi et al., *(3)*. Thermal decomposition of MPAN and PAN and reaction of the precursor MPA and PA radicals, respectively, with NO, HO_2 and RO_2 are similar as these reactions have been shown to be independent of the alkyl chain *(4)*. In the atmosphere, the MPAN lifetime is dependent on OH concentrations while the PAN lifetime is not as a result of the MPAN + OH reaction rate being 3 orders of magnitude faster than PAN + OH *(5, 6)*. The lifetimes of PAN and MPAN can be described by:

(Eq. S1) $$\tau_{MPAN} = \frac{1}{(k_{MPAN}(1-\beta)+k_{MPAN+OH}[OH])}$$

(Eq. S2) $$\tau_{PAN} = \frac{1}{(k_{PAN}(1-\beta)+k_{PAN+OH}[OH])}$$

where, k_{MPAN} and k_{PAN} are the rate constants for the thermal decomposition of MPAN and PAN, respectively. $k_{MPAN+OH}$ and k_{PAN+OH} are the rate constants for the OH oxidation

of MPAN and PAN, respectively. The β terms describes the branching ratio of the reformation of PAN or MPAN from their corresponding PA radicals relative to the loss of PA to the reaction with NO, HO_2 and RO_2 and is defined by:

(Eq. S3) $$\beta = \frac{1}{(1+(k_{PA+NO}[NO]+k_{PA+HO2}[HO_2]+k_{PA+RO2}[RO_2])/(k_{PA+NO2}[NO_2]))}$$

Figure S7 (supporting information) shows the increased importance of the OH reaction pathway to the MPAN lifetime at lower temperatures, e.g., at a temperature of 10 °C an increase in OH concentrations from 1×10^6 to 3×10^6 molecules cm^{-3} halves the MPAN lifetime while the same change in OH concentrations at 25 °C has a negligible effect on the MPAN lifetime.

In 2007, NO was not measured and was inferred by assuming a photostationary state relationship between NO_2, ozone and total peroxy radicals (HO_2+RO_2):

(Eq. S4) $$[NO] = \frac{J_{NO2}[NO_2]}{(k_{HO2+NO}[HO_2]+k_{RO2+NO}[RO_2]+k_{NO+O3}[O_3])}$$

The photolysis rate of J_{NO2} was determined from the Tropospheric Ultraviolet and Visible Radiation (TUV) model *(7)* for varying solar zenith angles at 30 minutes intervals for both BEARPEX campaigns while holding other parameters constant (cloud optical depth = 0; aerosol optical depth = 0.235; ozone column = 300 dobson units; single scattering aerosol albedo = 0.99), similar to previous work *(3)*. The output of the TUV model was scaled by PAR to account for periods of occasional cloud cover.

The RO_2 concentrations were estimated through a separate steady state relationship:

(Eq. S5) $$[RO_2] = \frac{\sum_i k_i[OH]VOC_i]}{(k_{HO2+RO2}[HO_2]+k_{NO+RO2}[NO]+2k_{RO2+RO2}[RO_2])}$$

The $\Sigma_i k_i[OH][VOC_i]$ term was constrained by measurements of the total OH reactivity. Equations 4 and 5 were solved iteratively until values of NO and RO_2 were obtained with convergence criteria of < 1 %.

The MAE production rate is given by:

(Eq. S6) $$MAE\ production\ rate = 0.2 * k_{MPAN+OH}[MPAN][OH]$$

The IEPOX production rate is given by:

(Eq. S7) $$IEPOX\ production\ rate = 0.75 * k_{ISOPOOH+OH}[ISOPOOH][OH]$$

In 2007, no calibrated ISOPOOH measurements were available so the IEPOX production rate was estimated based on the linear relationship between the production rate of ISOPOOH to the IEPOX production rate in 2009. Assuming the ISOPOO radicals are in steady state the production rate of ISOPOOH is given by:

(Eq. S8)

$$ISOPOOH\ production\ rate = 0.7 * k_{isoprene+OH}[isoprene][OH]$$

All the rate constants relevant to this work are shown in Table S1.

Table S1. Table of rate constants (cm^3 $molecules^{-1}$ s^{-1}) used for the APN steady state modeling analysis and determination of MAE and IEPOX production rates.

Reaction	K (T) or k (T,[M])[a]	Reference
$RC(O)O_2 + NO_2 \rightarrow APN$	$k_0=2.7x10^{-28}(T/300)^{-7.1}$ $k_\infty=1.2x10^{-11}(T/300)^{-0.9}$ $F_{cent}=0.3$ N=1	*(8, 9)*
$APN \rightarrow RC(O)O_2 + NO_2$	$k_0=4.9x10^{-3}exp(-12100/T)$ $k_\infty=4.0x10^{16}exp(-13600/T)$ $F_{cent}=0.3$ N=1.41	*(8, 9)*
$RC(O)O_2 + NO \rightarrow$ products	$8.1x10^{-12}exp(270/T)$	*(8, 9)*
$RC(O)O_2 + HO_2 \rightarrow$ products	$4.3x10^{-13}exp(1040/T)$	*(10, 11)*[b]
$RC(O)O_2 + RO_2 \rightarrow$ products	$2.0x10^{-12}exp(500/T)$	*(12)*
PAN + OH → products	$3.0x10^{-14}$ [c]	*(5)*
MPAN + OH → products	$3.2x10^{-11}$ [d]	*(6)*
$HO_2 + RO_2$	$2.9x10^{-13}exp(1300/T)$	*(10, 11)*[b]
$RO_2 + RO_2$	$2.4x10^{-12}$ [c]	*(10, 11)*[b]
$NO + RO_2$	$2.54x10^{-13}exp(360/T)$	*(10, 11)*[b]
$NO + HO_2$	$3.5x10^{-12}exp(250/T)$	*(13)*
$NO + O_3$	$3.0x10^{-12}exp(-1500/T)$	*(13)*
ISOPOOH + OH → IEPOX	$2.9x10^{-13}exp(1300/T)$	*(14)*
isoprene + OH → products	$2.7x10^{-11}exp(390/T)$	*(15)*

[a] $Where\ k(M) = \frac{k_0[M]}{1+\frac{k_0[M]}{k_\infty}} \times F_c$ and $\log(F_c) = \frac{log(F_{cent})}{1+\left(\frac{log(k_0[M]k_\infty)}{N}\right)^2}$

[b] Information was taken from the Master Chemical Mechanism, MCM v3.2, via website: http://mcm.leeds.ac.uk/MCM.

[c] At 298 K, though negligible temperature dependence expected.

[d] At 275 K, though negligible temperature dependence expected.

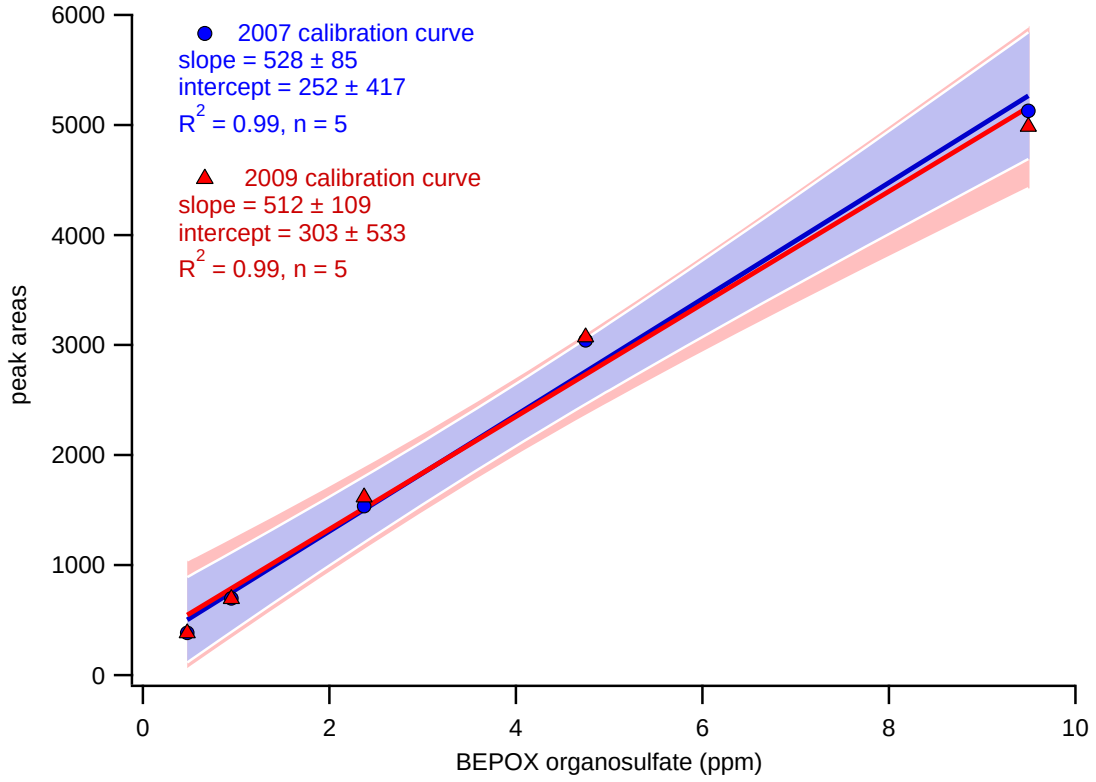

Figure S1. Calibration response curves for the BEPOX organosulfate (1,3,4-trihydroxybutan-2-yl hydrogen sulfate) used to calibrate the IEPOX- and MAE-derived organosulfates. Uncertainties in slope and intercepts are 95 % confidence intervals which are shown as the shaded areas.

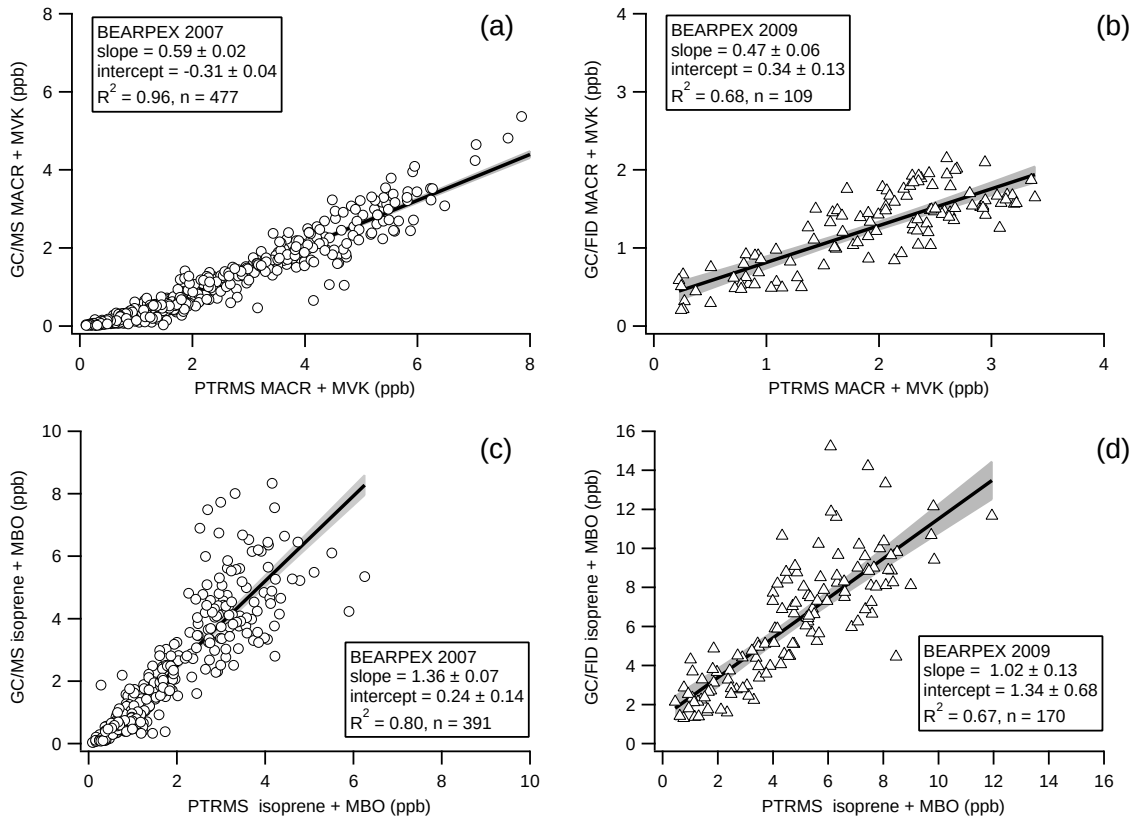

Figure S2. Intercomparison of sum of methacrolein and methyl vinyl ketone (MACR + MVK measured by GC/MS (NOAA) in 2007 (a) and by GC/FID (TAMU) in 2009 (b) to PTRMS measurements of m/z 71 (sum of MVK + MACR). Intercomparison of the sum of isoprene and MBO measured by GC/MS (NOAA) in 2007 (c) and by GC/FID (TAMU) in 2009 (d) to PTRMS measurements of m/z 69 (sum of isoprene and MBO) filtered to remove the early morning periods when the MBO contribution was dominant *(16)*. All of the 2007 campaign data was used in these comparisons. Similarity in the slopes (< 30 %) between the two campaigns indicates the NOAA and TAMU calibration scales were approximately in agreement and data can be compared directly between the campaigns.

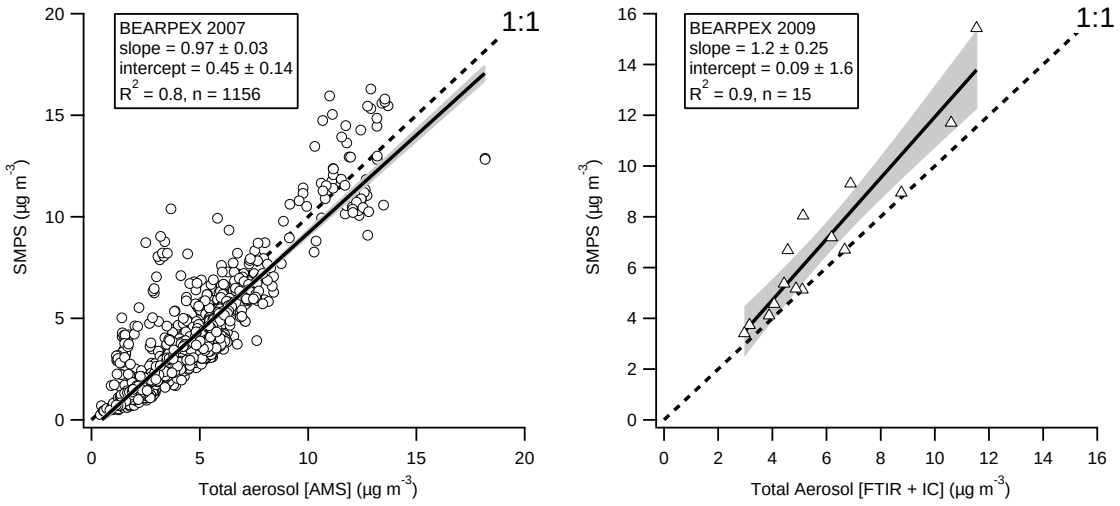

Figure S3. Intercomparison of total aerosol mass (µg m^{-3}) measured by SMPS and AMS (sum of organics, sulfate, nitrate, ammonium and chloride) during BEARPEX 2007 (left panel) and SMPS and the sum of FTIR organics and ion chromatogram (IC) measurements of sulfate, nitrate, ammonium and chloride during BEARPEX 2009 (right panel). SMPS mass was calculated assuming an aerosol density of 1.4 g cm^{-3}. This value was similar to SOA formed from monoterpene ozonoylsis *(17)* and within the range reported for ambient measurements *(18, 19)*.

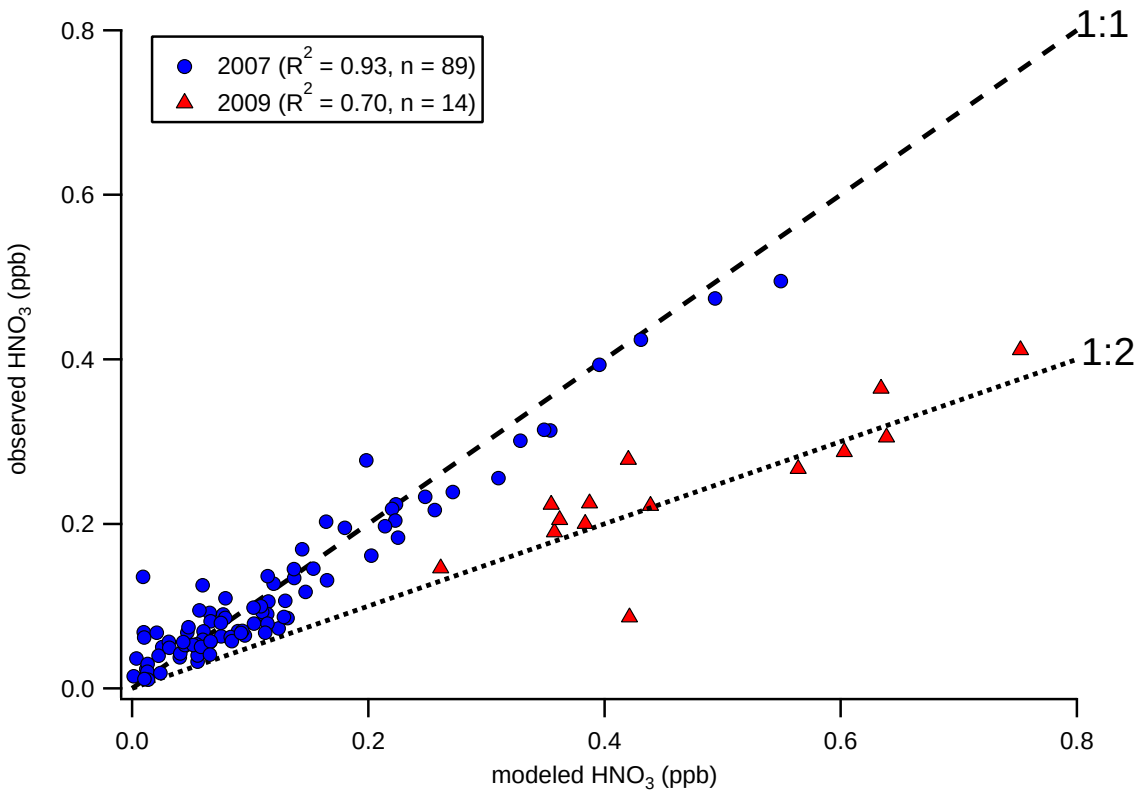

Figure S4. Comparison of observed and modeled (E-AIM) gas phase nitric acid during both BEARPEX campaigns (circles 2007; triangles 2009).

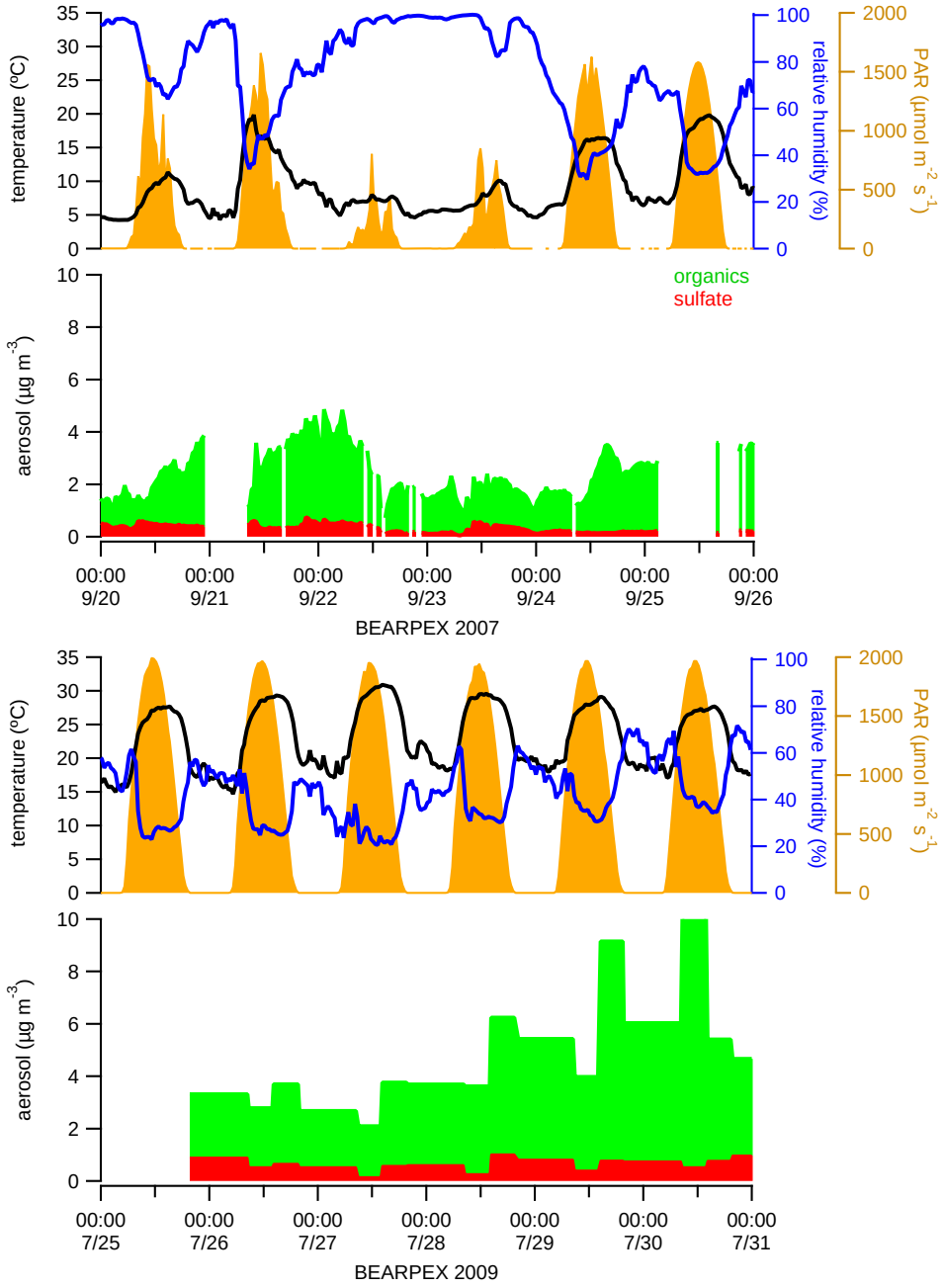

Figure S5. Intercomparison of temperature, relative humidity, photosynthetically active radiation (PAR), organic and sulfate aerosol concentrations (stacked abundances) for the filter collection periods during BEARPEX 2007 (top panel) and 2009 (bottom panel). In 2007 the organic and sulfate aerosol measurements were made by the AMS with a $PM_{1.0}$ size cut. While in 2009 they were made by FTIR and IC measurements and had a size cut of $PM_{2.5}$. Both datasets agree well with SMPS measurements suggesting minimal influence of the differing sampling cut points (see Figure S3).

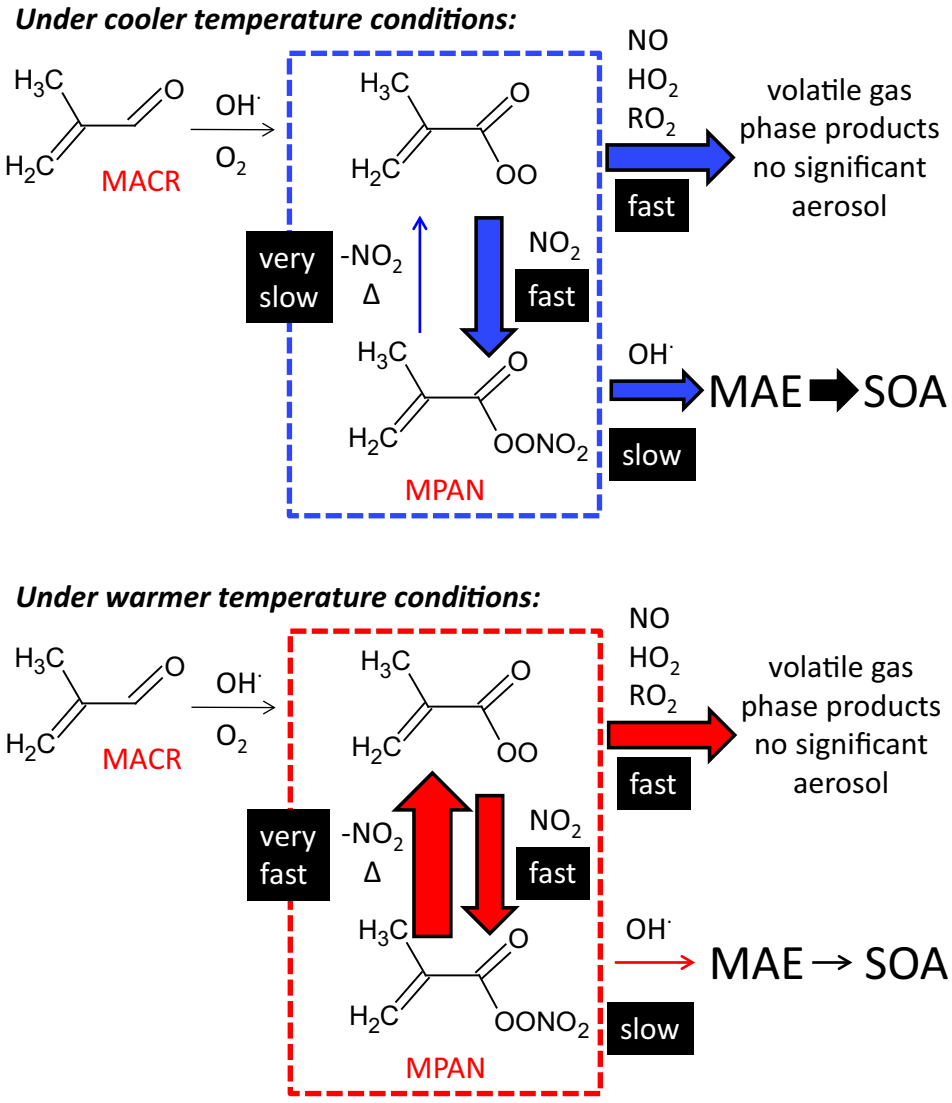

Figure S6. Schematic showing the temperature dependence of MPAN formation and loss and the formation of SOA through the MPAN + OH channel (adapted from *(3)*). The arrows are sized to approximately indicate the mass flux for the various reactions.

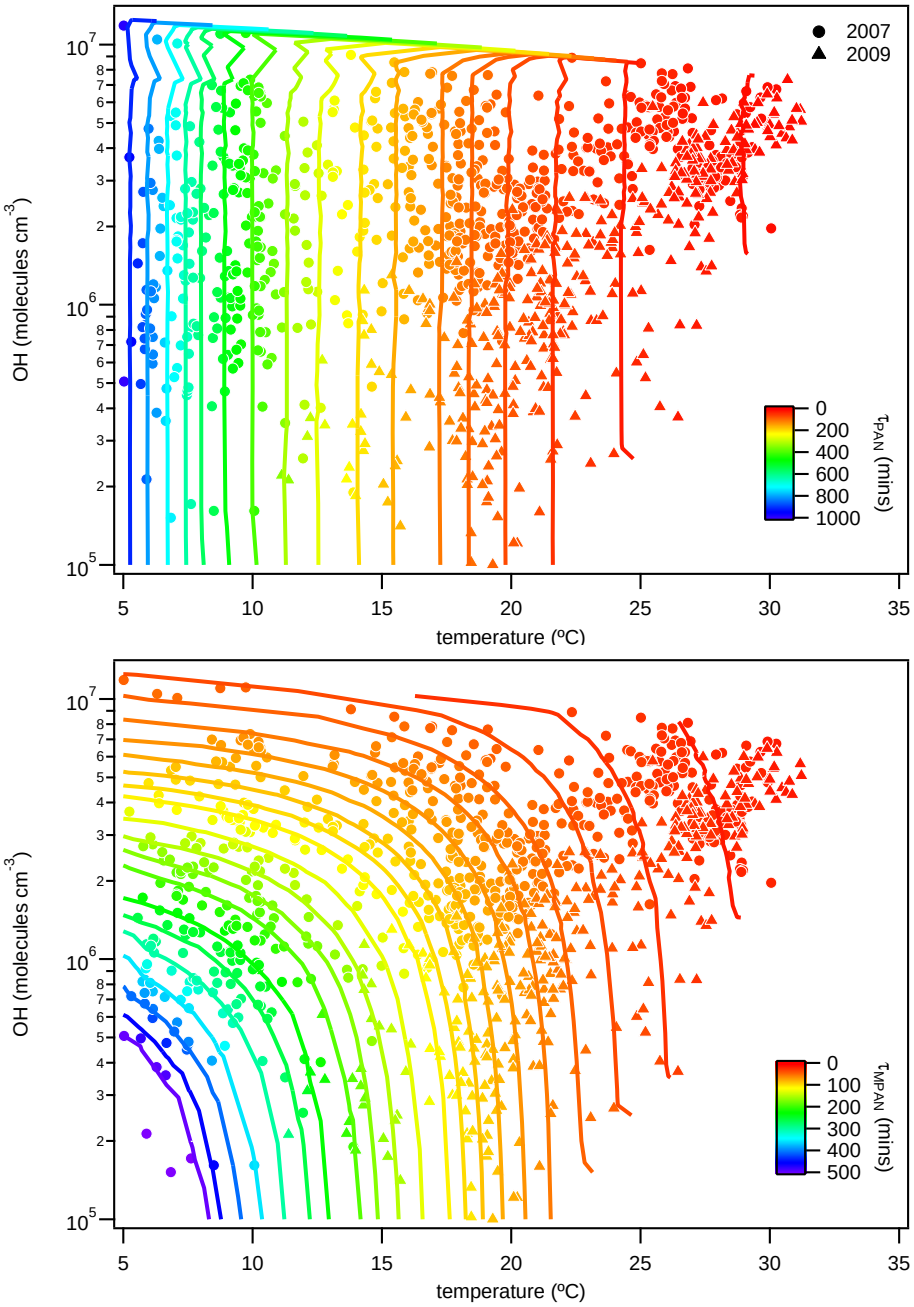

Figure S7. Modeled lifetimes of PAN (τPAN, upper panel) and MPAN (τMPAN, lower panel) as a function of ambient temperature and hydroxyl radical (OH) concentrations. The isopleths represent linear interpolations of the steady state APN model output (circles 2007, triangles 2009).

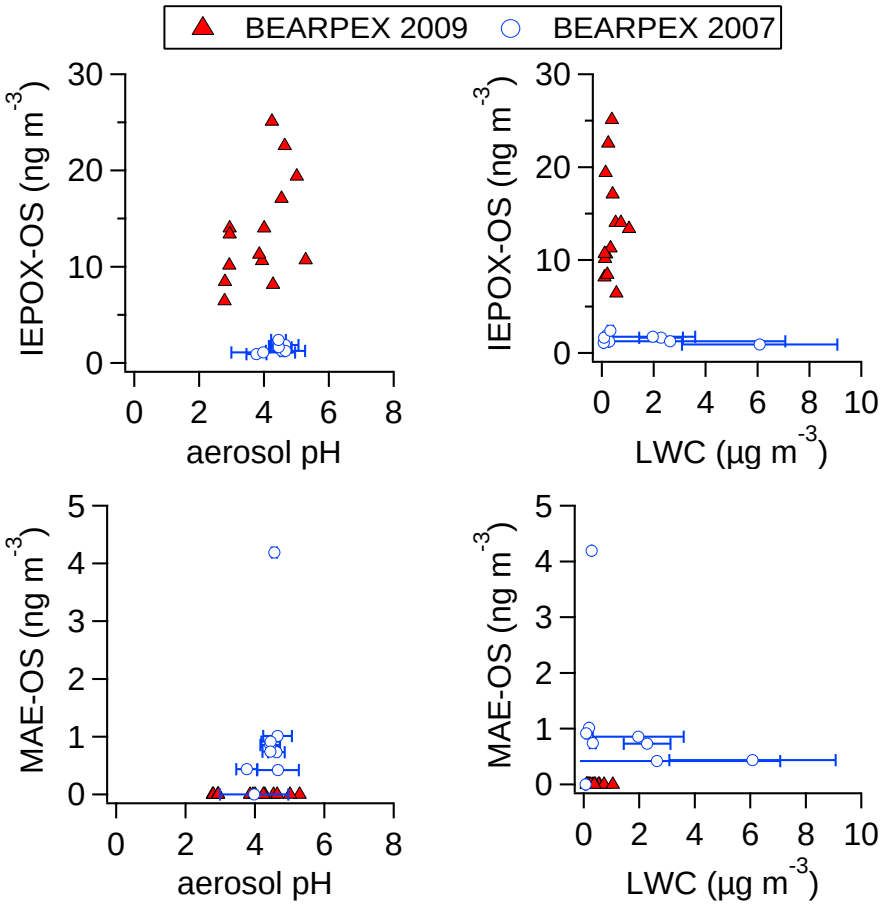

Figure S8. Correlations of the IEPOX- and MAE-derived organosulfates (IEPOX-OS and MAE-OS) to aerosol pH and liquid water content (LWC) for BEARPEX 2007 (open blue circles) and 2009 (filled red triangles). Aerosol pH and LWC were calculated using E-AIM. X-axis error bars reflect the interquartile range of the 30 minute data that was averaged to the filter timescale.

Figure S9. Comparison of the relative contribution of loss processes (F_{loss}) for gas phase MAE (left panel) and IEPOX (right panel) as a function of deposition velocity for both BEARPEX campaigns (pH = 4, LWC = 1 μg m^{-3}, OH = 2.8×10^{6} molecules cm^{-3}, T=11 °C and boundary layer height = 600m for 2007 and pH = 4, LWC = 0.1 μg m^{-3}, OH = 3.0×10^{6} molecules cm^{-3}, T=28 °C and boundary layer height = 700m for 2009).

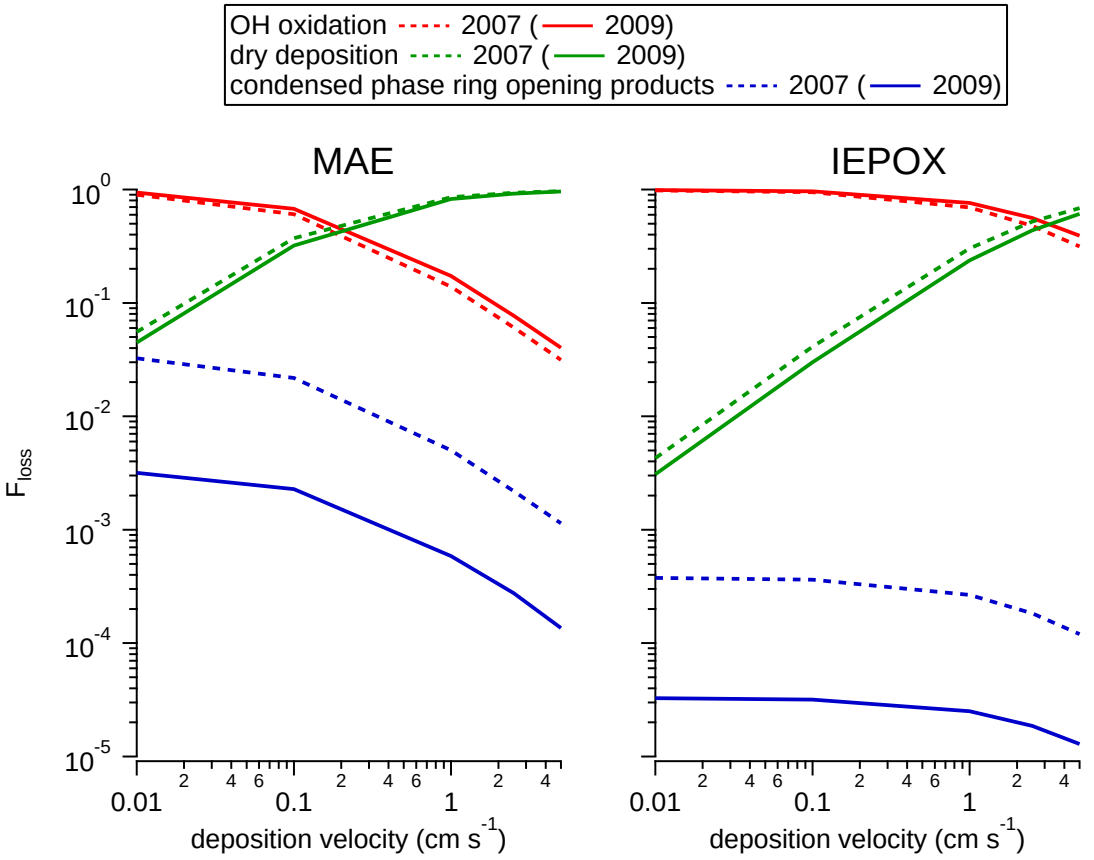

References

1. Worton, D. R.; Goldstein, A. H.; Farmer, D. K.; Docherty, K. S.; Jimenez, J. L.; Gilman, J. B.; Kuster, W. C.; de Gouw, J.; Williams, B. J.; Kreisberg, N. M.; Hering, S. V.; Bench, G.; McKay, M.; Kristensen, K.; Glasius, M.; Surratt, J. D.; Seinfeld, J. H. Origins and composition of fine atmospheric carbonaceous aerosol in the Sierra Nevada Mountains, California. *Atmos. Chem. Phys.* **2011,** *11* (19), 10219-10241.
2. Mao, J.; Ren, X.; Zhang, L.; Van Duin, D. M.; Cohen, R. C.; Park, J. H.; Goldstein, A. H.; Paulot, F.; Beaver, M. R.; Crounse, J. D.; Wennberg, P. O.; DiGangi, J. P.; Henry, S. B.; Keutsch, F. N.; Park, C.; Schade, G. W.; Wolfe, G. M.; Thornton, J. A.; Brune, W. H. Insights into hydroxyl measurements and atmospheric oxidation in a California forest. *Atmos. Chem. Phys.* **2012,** *12* (17), 8009-8020.
3. LaFranchi, B. W.; Wolfe, G. M.; Thornton, J. A.; Harrold, S. A.; Browne, E. C.; Min, K. E.; Wooldridge, P. J.; Gilman, J. B.; Kuster, W. C.; Goldan, P. D.; de Gouw, J. A.; McKay, M.; Goldstein, A. H.; Ren, X.; Mao, J.; Cohen, R. C. Closing the peroxy acetyl nitrate budget: observations of acyl peroxy nitrates (PAN, PPN, and MPAN) during BEARPEX 2007. *Atmos. Chem. Phys.* **2009,** *9* (19), 7623-7641.
4. Roberts, J. M.; Bertman, S. B. The thermal decomposition of peroxyacetic nitric anhydride (PAN)and peroxymethacylic nitric anhydride (MPAN). *International Journal of Chemical Kinetics* **1992,** *24* (3), 297-307.
5. Talukdar, R. K.; Burkholder, J. B.; Schmoltner, A. M.; Roberts, J. M.; Wilson, R. R.; Ravishankara, A. R. Investigation of the loss processes for peroxyacetyl nitrate in the atmosphere - UV photolysis and reaction with OH. *J. Geophys. Res.-Atmos.* **1995,** *100* (D7), 14163-14173.
6. Orlando, J. J.; Tyndall, G. S.; Bertman, S. B.; Chen, W. C.; Burkholder, J. B. Rate coefficient for the reaction of OH with CH_2=C(CH_3)C(O)OONO_2 (MPAN). *Atmos. Environ.* **2002,** *36* (11), 1895-1900, Pii s1352-2310(02)00090-0.
7. Madronich, S. Photodissociation in the atmosphere. 1. Actinic flux and the effects of ground reflections and clouds. *J. Geophys. Res.-Atmos.* **1987,** *92* (D8), 9740-9752.
8. Atkinson, R.; Baulch, D. L.; Cox, R. A.; Crowley, J. N.; Hampson, R. F.; Hynes, R. G.; Jenkin, M. E.; Rossi, M. J.; Troe, J. Evaluated kinetic and photochemical data for atmospheric chemistry: Volume I - gas phase reactions of O-x, HOx, NOx and SOx species. *Atmos. Chem. Phys.* **2004,** *4*, 1461-1738.
9. Atkinson, R.; Baulch, D. L.; Cox, R. A.; Hampson, R. F.; Kerr, J. A.; Rossi, M. J.; Troe, J. Evaluated kinetic and photochemical data for atmospheric chemistry: Supplement VI - IUPAC subcommittee on gas kinetic data evaluation for atmospheric chemistry. *Journal of Physical and Chemical Reference Data* **1997,** *26* (6), 1329-1499.
10. Jenkin, M. E.; Saunders, S. M.; Pilling, M. J. The tropospheric degradation of volatile organic compounds: A protocol for mechanism development. *Atmos. Environ.* **1997,** *31* (1), 81-104.
11. Saunders, S. M.; Jenkin, M. E.; Derwent, R. G.; Pilling, M. J. Protocol for the development of the Master Chemical Mechanism, MCM v3 (Part A): tropospheric degradation of non-aromatic volatile organic compounds. *Atmos. Chem. Phys.* **2003,** *3*, 161-180.
12. Tyndall, G. S.; Cox, R. A.; Granier, C.; Lesclaux, R.; Moortgat, G. K.; Pilling, M. J.; Ravishankara, A. R.; Wallington, T. J. Atmospheric chemistry of small organic peroxy radicals. *J. Geophys. Res.-Atmos.* **2001,** *106* (D11), 12157-12182.

13. NASA Chemical kinetics and photochemical data for use in atmospheric studies evaluation number 15, http://jpldataeval.jpl.nasa.gov. (September 14th, 2012).
14. Paulot, F.; Crounse, J. D.; Kjaergaard, H. G.; Kuerten, A.; St Clair, J. M.; Seinfeld, J. H.; Wennberg, P. O. Unexpected Epoxide Formation in the Gas-Phase Photooxidation of Isoprene. *Science* **2009,** *325* (5941), 730-733.
15. Atkinson, R.; Arey, J. Atmospheric degradation of volatile organic compounds. *Chemical Reviews* **2003,** *103* (12), 4605-4638.
16. Zhang, H.; Worton, D. R.; Lewandowski, M.; Ortega, J.; Rubitschun, C. L.; Park, J.-H.; Kristensen, K.; Campuzano-Jost, P.; Day, D. A.; Jimenez, J. L.; Jaoui, M.; Offenberg, J. H.; Kleindienst, T. E.; Gilman, J.; Kuster, W. C.; de Gouw, J.; Park, C.; Schade, G. W.; Frossard, A. A.; Russell, L.; Kaser, L.; Jud, W.; Hansel, A.; Capellin, L.; Karl, T.; Glasius, M.; Guenther, A.; Goldstein, A. H.; Seinfeld, J. H.; Gold, A.; Kamens, R. M.; Surratt, J. D. Organosulfates as Tracers for Secondary Organic Aerosol (SOA) Formation from 2-Methyl-3-Buten-2-ol (MBO) in the Atmosphere. *Environmental Science & Technology* **2012,** *46* (17), 9437-9446.
17. Kostenidou, E.; Pathak, R. K.; Pandis, S. N. An algorithm for the calculation of secondary organic aerosol density combining AMS and SMPS data. *Aerosol Science and Technology* **2007,** *41* (11), 1002-1010.
18. Khlystov, A.; Stanier, C.; Pandis, S. N. An algorithm for combining electrical mobility and aerodynamic size distributions data when measuring ambient aerosol. *Aerosol Science and Technology* **2004,** *38*, 229-238.
19. Stein, S. W.; Turpin, B. J.; Cai, X. P.; Huang, C. P. F.; McMurry, P. H. Measurements of relative humidity dependent bounce and density for atmospheric particles using the DMA impactor technique. *Atmos. Environ.* **1994,** *28* (10), 1739-1746.